Chapter

Generation and Relaxation of Residual Stresses in Automotive Cylinder Blocks

Serageldin Salem Mohamed, Agnes M. Samuel, Herbert W. Doty, Salvador Valtierra and Fawzy H. Samuel

Abstract

There is direct proportionality between ultimate tensile stress (UTS) and residual stresses (RS). Residual stresses gradually decrease with decreasing cooling/quenching rates. Quenching in cold water develops highest, whereas air cooling produces lowest, residual stresses. Significant increase in RS is observed in specimens with low dendrite arm spacing (high solidification rate), while lower residual stresses are measured in specimens with high dendrite arm spacing (low solidification rate). For I-4 and V-6 engine blocks, there is refinement in microstructure due to the increase in solidification rate along the cylinder length. The developed residual stresses are normally tensile in both engine types. Air cooling following solution heat treatment produces higher RS compared to warm water and cold water quenching. Solution heat treatment and freezing lead to maximum RS relaxation where 50% of the stresses are reduced after the solution heat treatment step. Aging time and temperature are directly proportional to the residual stresses relaxation. Relaxation of RS also depends on the geometry and size of the workpiece. It should be mentioned here that the I-4 and V-6 cylinder blocks were provided by Nemak-Canada (Windsor-Ontario-Canada). Residual stress measurements technique and procedure are typical of those used by the automotive industry in order to provide reliable data for industrial applications supported by intensive experiments.

Keywords: residual stresses, Al cylinder blocks, stress relaxation, effect of microstructure, heat treatment, quenching conditions

1. Introduction

Residual stress is generally referred as an internal stress, which exists in equilibrium inside a component in the absence of any external forces or constraints, temperature gradients, or any other external influences [1]. Any existing residual stresses are considered as elastic stresses that are kept under static equilibrium. Elastic limit is the maximum value that can be reached by any residual stresses. Any stresses higher than the value of elastic limit with no opposing forces will be relieved by plastic deformation until it reaches the value of the yield stress [2].

Excessive residual stresses may be generated due to the large difference in thermal expansion coefficient between the aluminum alloy ($2.4 \times 10^{-5}\ K^{-1}$) and cast iron ($1.5 \times 10^{-5}\ K^{-1}$) [3]. The presence of these residual stresses renders engine

blocks prone to either distortion or failure. Distortion of the cylinder bores results in a loss in compression of the air-fuel mixture due to improper sealing between the cylinder wall and the piston. This loss of sealing causes a portion of the compressed air-fuel mixture to leak out of the combustion chamber by a process known as "blow-by" [4] which reduces the engine efficiency. In conclusion, aluminum engine blocks with gray iron cylinder liners are prone to tensile residual stresses along the cylinder bores, which results in distortion, cracks, and a reduction in engine efficiency. Several ideas have been introduced in order to change the cast iron liners with another suitable replacement but due to technical and economic problems cast in liners are considered the most effective option in engine block manufacturing [5].

Many automobile parts are made of aluminum alloys such as engine blocks, cylinder heads, and suspension parts, and to perform efficiently and eliminate premature failure, residual stresses must be minimized. During service, these parts undergo heating and cooling cycles which promote residual stresses. Presence of residual stresses in the casting deteriorates fatigue life and dimensional stability of the part [6]. Tensile residual stresses can result in distortion and cracking of the component during quenching or machining and if this occurs during service, it can cause a reduction in efficiency or failure of the part [7]. The presence of residual stresses and/or distortion in a structural component, such as an aluminum casting, has a negative influence on the component's dimensional tolerance, performance and fatigue life [6].

Dynamic simulation was conducted on two crankshafts, cast iron and forged steel, from similar single cylinder four stroke engines [8]. Finite element analysis was done for different engine speeds and as a result, critical engine speed and critical region on the crankshafts were obtained. Stress variation over the engine cycle and the effect of torsional load in the analysis were investigated. Results from FE analysis were verified by strain gages attached to several locations on the forged steel crankshaft. Modeling of residual stresses in quenched cast aluminum components was carried out by Wang et al. [9]. To simulate residual stress and distortion induced during quenching, a finite element based approach was developed by coupling an iterative zone-based transient heat transfer algorithm with material thermo-viscoplastic constitutive model. With the integrated models, the numeric predictions of residual stresses and distortion in the quenched aluminum castings are in a good agreement with experimental measurements.

The automotive industry is the largest consumer of Al-Si cast alloys, where these alloys have replaced steel for the sake of greater fuel efficiency and higher performance, attributed to their much lighter weight and high thermal conductivity. Thus, Al-Si castings have gradually replaced automobile parts such as transmission cases, intake manifolds, engine blocks and cylinder heads that were formerly manufactured using steel and cast iron. The most common aluminum casting alloys that are used in the automotive industry are 319.0 (Al-6Si-3.5Cu), 332.0 (Al-9.5Si-3Cu-l.0Mg), 355.0 (Al-5Si-l.3Cu-0.5Mg), A356.0 (Al-7Si-0.3Mg), A357.0 (Al-7Si-0.5Mg), 380.0 (Al-8.5Si-3.5Cu), 390.0 (Al-17.0Si-4.5Cu-0.6Mg), 413.0 (Al-12Si) and 443.0 (Al-5.2Si) alloys. Amounts of alloying elements differ between different series, leading to changes in the final properties [5, 8].

Residual stresses can be classified into two groups according to their origin: the first one is macroscopic residual stresses which correspond to the residual stresses originating from heat treatment, machining, and mechanical processing, while the second group is microscopic residual stresses which often originate from lattice defects such as vacancies, dislocation pile-ups and thermal expansion/contraction mismatch between phases and constituents, or from phase transformations [6, 9].

The magnitude of residual stress depends on the stress-strain behavior and the degree of the temperature gradient attained during the quenching operation, which produces strain mismatch. It is found that the magnitude of the residual stresses is

directly proportional to the yield stress and Young's modulus (E). Furthermore, the stress-strain behavior at elevated temperature is an important factor in determining the amount of residual stresses [2]. Certain physical properties also increase the amount of strain mismatch (residual stresses) such as low thermal conductivity (k), high specific heat (c), high coefficient of thermal expansion (α) and high density (ρ) [2].

Residual stresses are often regarded as undesirable and harmful. Prolonging service life of any product can be achieved if such harmful residual stresses are eliminated or reduced. Several methods have been introduced in order to reduce these residual stresses. Annealing is one of these methods which involves exposing the material to very slow rates of cooling and heating with the aim of relieving stresses without altering the microstructure. If the temperature is too high then recrystallization might happen, leading to change in properties such as the yield stress which may not be desirable. The residual stresses relaxation by annealing occurs by one of two main mechanisms. The first is plasticity caused by reduced yield strength at an elevated temperature where instantaneous relief of stress occurs as the temperature is increased. The second mechanism is a creep based mechanism, which allows stress relief to occur over time [1].

Residual stresses can be quantified by many techniques. There are mechanical techniques such as sectioning, hole-drilling, curvature measurements, and crack compliance methods. These techniques correlate the measured residual stresses in components to the distortion. Diffraction techniques cover electron diffraction, X-ray diffraction, and neutron diffraction, which quantify the residual stresses by measuring the elastic strains in components. Other techniques, including magnetic and ultrasonic techniques, and piezo spectroscopy are also used to measure the residual stresses developed [6]. The mechanical techniques are considered destructive tests while the others are non-destructive tests but their accuracy is dependent on the microstructural variation and geometric complexity of the component structure.

An engine block as shown in **Figure 1** is the largest metal component in a car and is the most intricate. It holds and supports all other engine components such as cylinders and pistons and contains passages for coolant. The engine block is where combustion converts into mechanical energy that drives transmission propelling the car. Engine blocks used to be made of iron but today most of them are made of

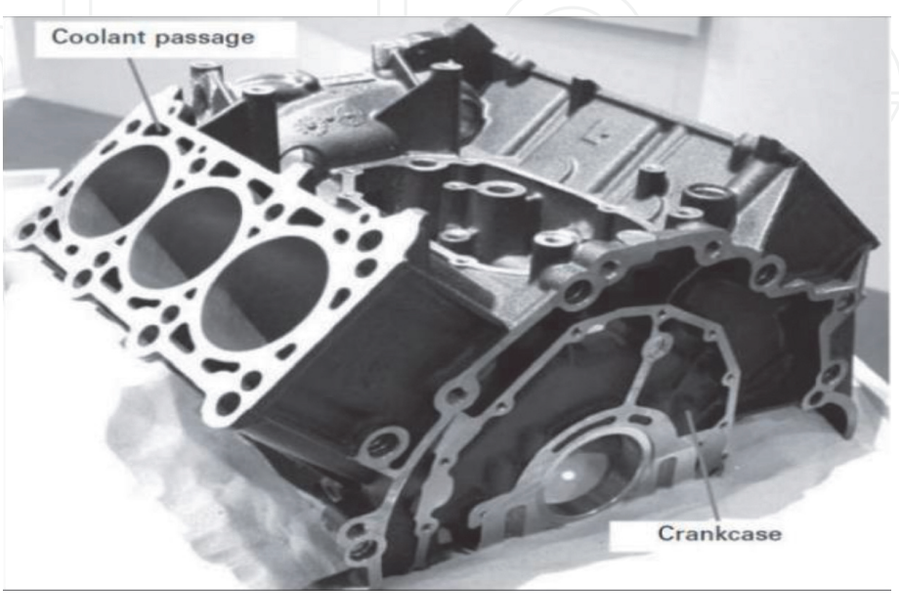

Figure 1.
Cast iron V-cylinder block (closed deck type) including a crankcase [10].

aluminum alloy for fuel efficiency. It is the largest and most complex single piece component in the car to which all other parts are attached. It represents from 3 to 4% of the total weight of the car. The block is typically arranged in a "V," inline, or I-4 horizontally-opposed (also referred to as flat) configuration and the number of cylinders may range from 3 to as much as 16 [10].

Carrera et al. [11] conducted a series of experimental tests to measure the residual stresses using strain gauges attached to different automotive engine blocks **Figure 2**. They discovered the development of tensile stresses higher than 150 MPa when the engine block contained the cast iron liners, while the engine blocks without cast iron liners exhibited 20 MPa compressive stresses in the cylinder bridge (**Table 1**). Furthermore, it has been observed that the residual stresses are affected by the dimension of the block and the wall thickness of the cylinder bridge where residual stresses decrease as the thickness increases. It was also found that V-8 engine blocks develop higher residual stresses than I-4 blocks with equivalent walls thickness [11]. These observations match the results for residual stresses obtained from the finite element model made by Su et al. [12].

Carrera et al. [13] and Colas et al. [14] analyzed residual stresses in complex aluminum castings. Measurements of residual stresses were carried out by extensometric means in automotive engine blocks. The results indicate that tensile stresses are caused during cooling of the aluminum alloy restricted by iron liners. Such observation is confirmed by measurements carried out in engine blocks cast without liners that develop compressive stresses in their cylinder bridges. The residual stresses are affected by the dimension of the block and the wall thickness of the interliner bridge, implying that a bigger block, such as a V-8 will develop higher

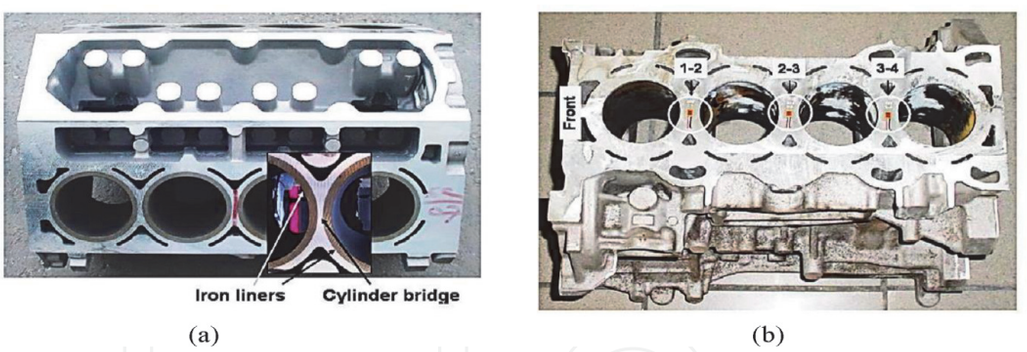

Figure 2.
Identification of the cylinder bridges in an I-4 block. Glued strain gauges are indicated: (a) eight cylinders and (b) four cylinder blocks.

Trial	Block	Weight (kg)	Wall thickness (mm)	Condition	Liners	Stress (MPa)	
						Average	Standard deviation
A	I-4	30.6	3.5	As-cast	Cast-in	113.8	3.5
B	I-4	30.6	3.5	T7	Cast-in	94.5	3.2
C	V-8	54.7	4.8	T7	Cast-in	121.8	9.9
D	V-8	56.2	3.0	T7	Cast-in	148.9	17.4
E	V-8	55.4	3.4	T7	Cast-in	158.7	14.6
F	V-8	43.5	8.5	T7	Inserted	–18.7	3.8

Table 1.
Characteristics of the studied blocks.

residual stresses than an I-4 that has walls of equivalent dimensions. Heat treating contribute to reduce the residual stresses.

A practice of shaking the blocks at an early stage contributes in reducing the residual stresses. Measurements of residual stresses in automotive blocks can be used as an early warning of changes taking place during processing of the material, and can be an aid when changes in design have to be made. According to Elmquist et al. [15], the feeders, which act as extra heat sources, affect residual stresses locally and helps to differences in stresses beneath the feeders, compared to corresponding areas between the feeders. **Table 2** lists the most frequently used alloys in the production of automotive components. Residual stresses as shown in **Figure 3** can be classified into two groups according to their origin: the first one is macroscopic residual stresses originating from heat treatment, machining, and mechanical processing. The second group is microscopic residual stresses which often originate from lattice defects.

2. Experimental procedure

The present work was divided into two parts: stage I aiming at evaluating the effect of metallurgical parameters on the residual stress in B319-based alloys and stage II measuring the residual stresses in I-4 and V-6 engine blocks using the information gathered from stage I.

2.1 Stage I

The chemical composition of the B319.1 base alloy coded E is shown in **Table 3**. The as-received ingots were melted in a 120-kg capacity SiC crucible, using an electrical resistance furnace. The melting temperature was maintained at 750 $\pm$ 5°C. Both alloy melts were grain refined and modified using Al-5% Ti-1%B and Al-10% Sr master alloys, respectively, to obtain levels of 0.25% Ti and 200 ppm Sr in the melt. Finally, the melts were degassed for ~15–20 min with a rotary graphite impeller rotating at ~130 rpm, using pure dry argon. Following this, the melt was carefully skimmed to remove oxide layers from the surface.

The melt was poured into different molds for various purposes, namely (a) ASTM B-108 permanent mold, for preparing the tensile test bars; (b) an L-shaped rectangular graphite-coated metallic mold; and (c) a block shaped graphite-coated metallic mold. All molds were preheated to 450°C to drive out moisture and avoid cold shut of the blocks. Regarding ASTM B-108 mold, each casting provides two test bars, with a gauge length of 70 mm and a cross-sectional diameter of 12.7 mm. Three samplings for chemical analysis were also taken simultaneously at the time of the casting; this was done at the beginning, in the middle, and at the end of the casting process to ascertain the exact chemical composition of each alloy.

The L-shaped mold and block castings were mainly used for residual stress measurements and microstructure samples and for preparing samples for micro-structural examination. The molds were preheated to 250°C. Samples were prepared for the measurement of secondary dendrite arm spacing (SDAS) and grain size in both alloys. Bars were cut from both molds with the dimensions of 200 $\times$ 40 $\times$ 40 mm^3 for measuring of residual stresses using the sectioning method. All the samples, tensile test bars for residual stress measurements treated. Tensile test bars were to the point of fracture using a servohydraulic mechanical testing machine (model 801 produced by MTS), at a strain rate of 4×10^{-4} s^{-1}.

Samples for microstructural characterization were used for secondary dendrite arm spacing (SDAS) and grain size measurements. For grain size measurements,

Aluminum foundry and die cast alloys														
A.A. No.	**Former commercial designation**	**Cu**	**Zn**	**Fe**	**Sl**	**Mn**	**Mg**	**Cr**	**Nl**	**Sn**	**Tl**	**Others**		**Al**
												Ea.	**Total**	
2081	108	3.5 4.5	1.0	0.9	2.5 3.50	0.50	0.10		0.35		0.25		0.50	Bal.
296.1	B295.0/B195	4.0 5.0	0.50	0.9	2.0 3.0	0.35	0.05		0.35		0.25		0.35	Bal.
319.1	319	3.0 4 0	1.0	0.8	5.5 6.5	0.50	0.10		0.35		0.25		0.50	Bal.
319.1sr		3.0 4.0	1.0	0.9	5.5 6.5	0.50	0.25 40		0.35		0.25	(1)	0.50	Bal.
355.1	355	1.0 1.5	0.35	0.50	4.5 5.5	0.50	0.45 0.6	0.25			0.25	0.05	0.15	Bal.
356.1	356	0.25	0.35	0.50	6.5 7.5	0.35	0.25 0.40				0.25	0.05	0.15	Bal.
A360.1	A360	0.6	0.40	1.0	9.0–10.0	0.35	0.45–0.6		0.50	0.15			0.25	Remainder
A380.1	A380	3.0–4.0	2.9	1.0	7.5–9.5	0.50	0.10		0.50	0.35			0.50	Remainder
B380.1		3.0–4.0	0.9	1.0	7.5–9.5	0.50	0.10		050	0.35			0.50	Remainder
383.1	383	2.0–3.0	2.9	1.0	9.5–11.5	0.50	0.10		0.30	0.15			0.50	Remainder
383-1		2.0–3.0	0.90	1.0	9.5–11.5	0.50	0.10		0.30	0.15			0.50	Remainder
384.1	384	3.0–4.5	2.9	1.0	10.5–120	0.50	0.10		0.50	0.35			0.50	Remainder
A384.1		3.0–4.5	0.9	1.0	10.5–12.0	0.50	0.10		0.50	0.35			0.50	Remainder
B390.1		4.0–5.0	1.4	1.0	16.0–18.0	0.50	0.50–0.65		0.10		0.20	0.10	0.20	Remainder
A413.1	13	1.0	0.40	1.0	11.0–13.0	0.35	0.10		0.50	0.15			0.25	Remainder
C443.1	43	0.6	0.40	1.1	4.5–6.0	0.35	0.10		0.50	0.15			0.25	Remainder

Aluminum foundry and die cast alloys														
A.A. No.	**Former commercial designation**	**Cu**	**Zn**	**Fe**	**Sl**	**Mn**	**Mg**	**Cr**	**Nl**	**Sn**	**Tl**	**Others**		**Al**
												Ea.	**Total**	
705.1	603, Ternalloy 5	0.20	2.7 3.3	0.6	0.20	0.40 0.6	1.5 1.8	0.20 0.40			0.25	0.05	0.15	Bal.
712.2	D712.2, D612, 40E	0.25	6.0 6.5	0.4	0.15	0.10	0.50 0.65	0.40 0.60			0.16 0.25	0.05	0.20	Bal.
713.1	613, Tenzaloy	0.40 1.0	7.0 8.0	0.8	0.25	0.6	0.25 0.50	0.36	0.15		0.25	0.10	0.25	Bal.

Table 2.
Aluminum foundry and die casting alloys (standard and custom specification aluminum ingots).

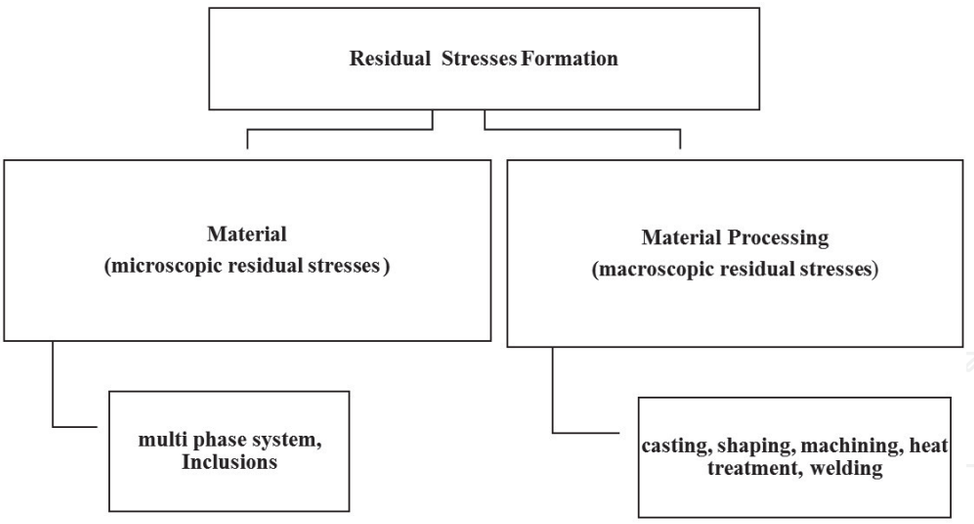

Figure 3.
Origin of residual stress formation.

Element wt.%	%Si	%Cu	%Fe	%Mn	%Mg	%Sr	%Ti	%Al
B319.1	7.4	3	0.4	0.2	0.26	0.05	0.26	Bal.

Table 3.
Chemical composition of the B319.1 alloy.

the polished samples were etched for 15 seconds, using a solution containing 2 ml HF (48%) + 3 ml HCl (conc.) + 5 ml HNO_3 (conc.) and 190 ml distilled water.

Residual stress measurements using the sectioning technique require block surface preparation and strain gauge installation prior to strain measurement and calculation of residual stress.

1. The block surface of the alloy is machined, and then abraded manually successively using SiC papers of grit size 120, 320 and 600.

2. Strain gage installation: place strain gauge (bonding side down) on a chemically clean and neutral plastic plate surface. It is important to mention that all strain measurements are performed at/under the same ambient temperature (23°C) and dry condition (humidity was less than 13%) (**Figure 4**).

2.2 Stage II

In this stage, the investigation will focus on the analysis of residual stresses evolved in I-4 and V-6 engine blocks following different types of heat treatments

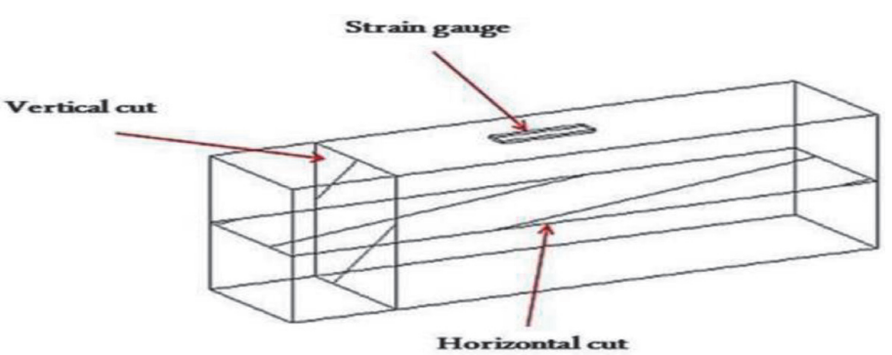

Figure 4.
Sketch illustrating cutting directions.

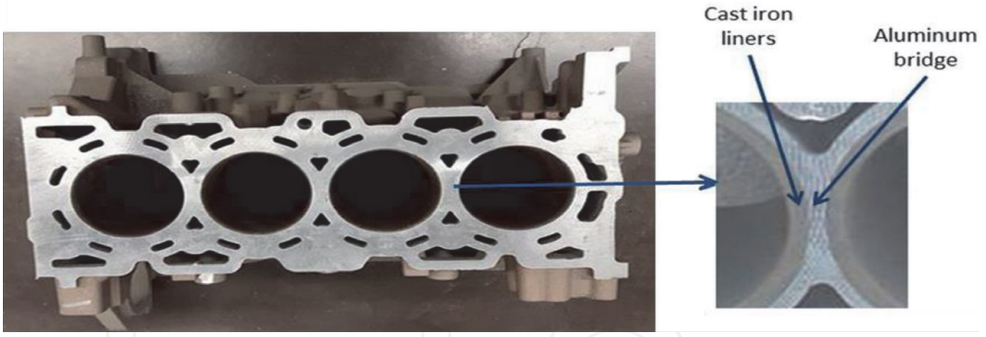

Figure 5.
I-4 engine block.

(solutionizing as well as artificial aging). The liners used in these blocks were preheated to 400°C using induction coils, prior to being inserted into the mold to promote a more uniform microstructure (**Figure 5**) [16].

The engine blocks followed solution heat treatment (SHT) at 500°C for 8 hours, then quenching/cooling in different media, prior to T6 and T7 aging treatment for various aging times. Two quenching media were applied: cold water, warm water. Artificial aging, T6 aging is carried out at for 10, 50 and 100 hours 170°C (T6 aging). As for T7 treatment, samples were aged at 250°C for 10, 50, and 100 hours aging times. The T7 treatment is used industrially. To facilitate the handling of the engine block in the foundry, the I4 engine blocks were cut in half. This procedure was carried out after validating that there would be no change in results between the whole block (four cylinders) and half the block (two cylinders).

The sectioning method is a complete destructive test and can be considered as the first proposed method for measuring residual stresses. It involves cutting of the component with an electric strain gauge attached, and relies on the measurement of local strain (using strain gages) induced due to the release of residual stress upon removal of material from the specimen [14–16].

3. Results and discussion

3.1 Stage I

Results of secondary dendrite arm spacing (SDAS—**Figure 6**) measurements show that the average SDAS for the block casting is 60 μm which is reflected by the large grain size observed in **Figure 7(a)**. Due to the high solidification rate obtained

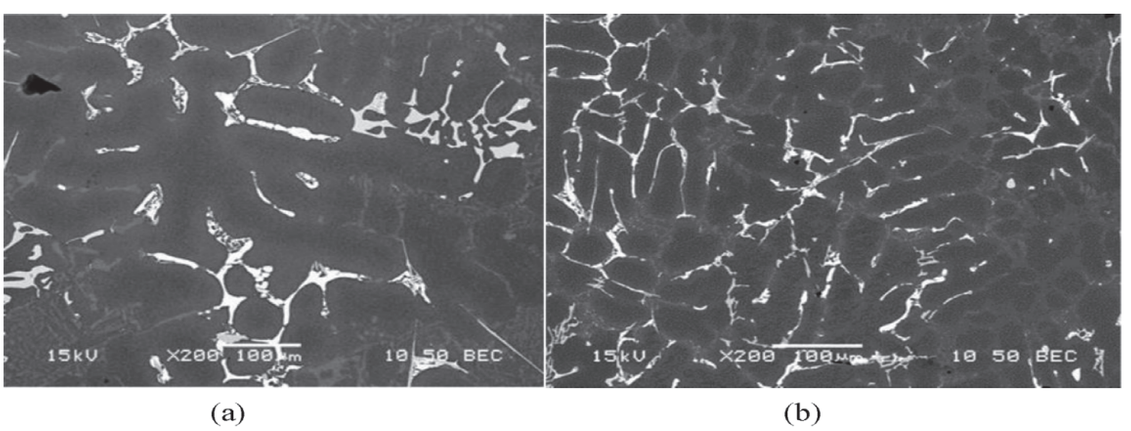

Figure 6.
Backscattered electron images of as cast B319.1 (a) block mold casting. (b) L-shaped mold casting.

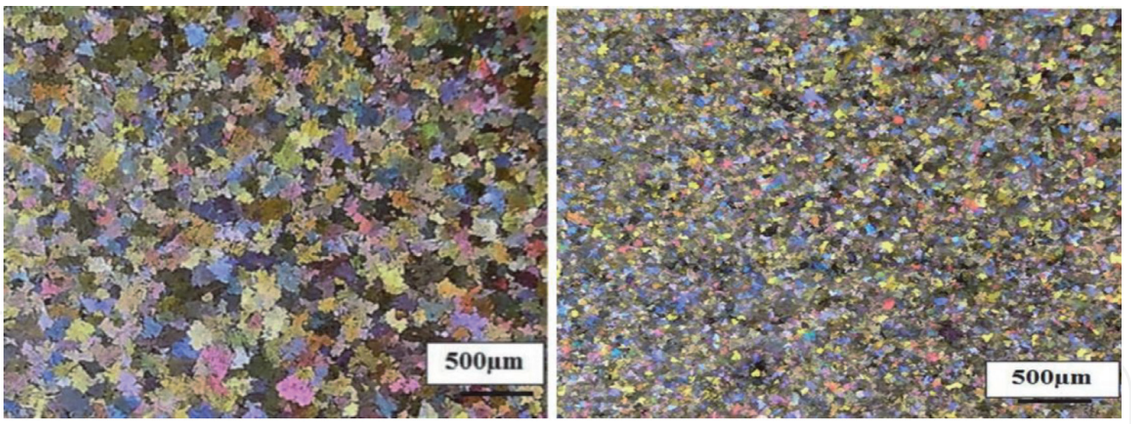

Figure 7.
Macrographs of B319.1 alloy for (a) block casting and (b) L-shaped casting.

with the L-shaped casting, the average SDAS was found to be 25 µm, as is also confirmed by the small grain size noted in **Figure 7(b)**.

From **Figure 8**, it will be observed that the strength values for the as-cast alloy samples of B319.1 exhibit UTS values of about 319 MPa. The B319.1 alloy contains Al, Si and Cu, and Mg and Fe as strengthening elements. The primary strengthening phases for B319.1 are the θ Al_2Cu phase and eutectic silicon. The alloying elements added to B319.1 enhanced both yield and tensile strength. The T6 temper allows for increased strength where it develops more stable mechanical properties with a corresponding loss of ductility. Aging at 170°C for 10 hours hardens the alloy, due to the formation of Guinier-Preston zones and coherent θ' Al2Cu phase particles [17–20]. Overaging can be done either at high temperatures or prolonged exposure at an intermediate temperature, and results in the simultaneous formation of relatively large, non-coherent θ' Al2Cu plates which act as hard non-shearable obstacles to dislocations. Such non-shearable particles lead to lower UTS but with high strain-hardening rate, due to the accumulation of Orowan loops around the strengthening particles. As the strain is increased, the buildup of primary shear loops generates intense stress fields around the strengthening precipitates. [21–23].

As coarsening occurs, the inter-particle spacing is widened which will have a direct effect on the dislocation motion. According to the Orowan relationship (**Figure 9**), larger inter-particle spacing results in a decrease in the resistance to

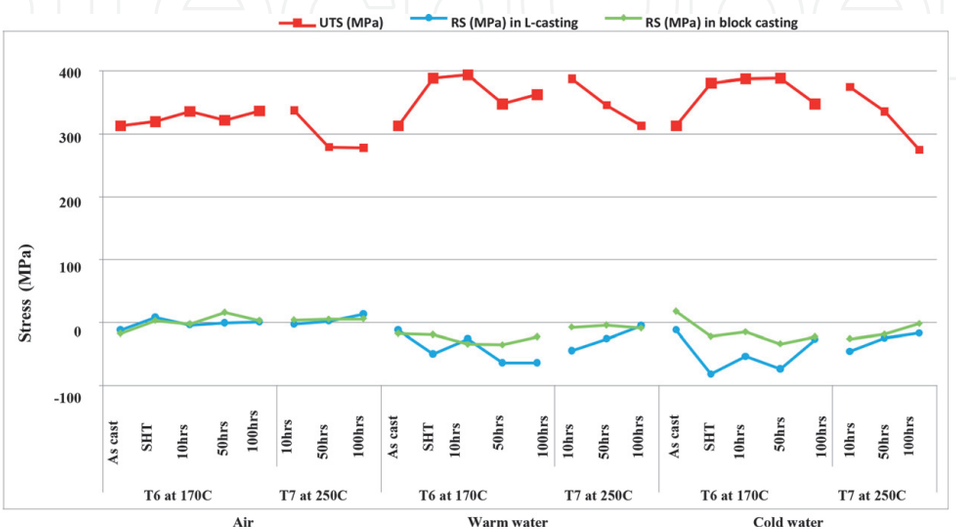

Figure 8.
Variation in YS, UTS and %El at different quenching rates and different aging parameters for B319.1 alloy.

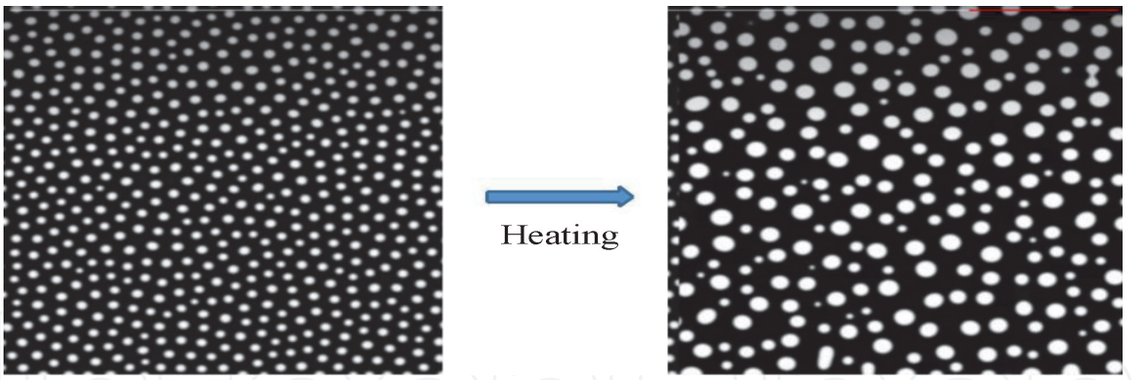

Figure 9.
Ostwald ripening mechanism: larger particles grow at the expense of the smaller particles [28].

dislocation motion thereby facilitating the occurrence of Orowan looping. The increased deformability of the matrix via the easy dislocation motions leads to reduced strength and subsequently diminished quality index values in the castings [24–30]. Aging at lower temperature results in formation of precipitates; with fine sizes, high density and lower inter-particle spacing. In this case, the precipitates provide strong resistance to dislocation motion and the occurrence of Orowan looping becomes difficult leading to a hardening of the materials and an increase in the overall strength, as shown in **Figure 8** [28].

Residual stresses (RS) are elastic accommodation of non-uniform plastic strains generated either thermally or by phase transformation. Generally, the hardness is inversely proportional to the square root of grain size (Hall-Petch equation). Greater the hardness, greater will be the residual stresses. Thus, it could be concluded that grain size has an inverse effect on residual stresses. In general, it is observed that the residual stresses measured are compressive in nature, and are generated due to the steep thermal gradient between core and outer layer at the start of the quenching/cooling process [10] as well the precipitation of complex phases such as α Al15(Mn,Fe)3Si2, β-Al5FeSi and CuAl2 in the B319.1 alloy [16, 31–33].

Generally, stress relief involves uniform heating of a part to a suitable temperature, holding at this temperature for a period of time, followed by slow cooling to prevent the reintroduction of thermal stresses, as stress relieving is highly dependent on the temperature. At high temperatures, such as those used in solution heat treatment, the material yield strength is remarkably reduced, causing plasticity mechanisms to relieve the elastic strain through rapid thermal activation of dislocations. It should be noted that at high temperature, major reduction in residual stresses can be encountered with major decrease in the properties of the material as the precipitates get coarser and lose their hardening capabilities during annealing at high temperatures [34–36]. In other words, heat-treatable aluminum alloys cannot be stress relieved by annealing as the temperature required to encourage stress relief will coincide with that which promotes the precipitation of the second phase constituents, so that stress relieving must be attained at a lower temperature (i.e. during aging).

The amount of residual stresses relieved through T6 treatment provides only modest reduction in residual stresses; while aging at 250°C causes at least 75% residual stress relaxation and can annihilate most locked-in residual stresses with increasing time. This behavior could be attributed to the fact that dislocation glide or climb occurs more readily at higher temperatures. Specimens with large SDAS (60 μm) were also found to be more prone to residual stress relief. In general, the increase in SDAS is found to reduce the amount of residual stresses that originate and facilitate residual stress relaxation which is related to the reduction of

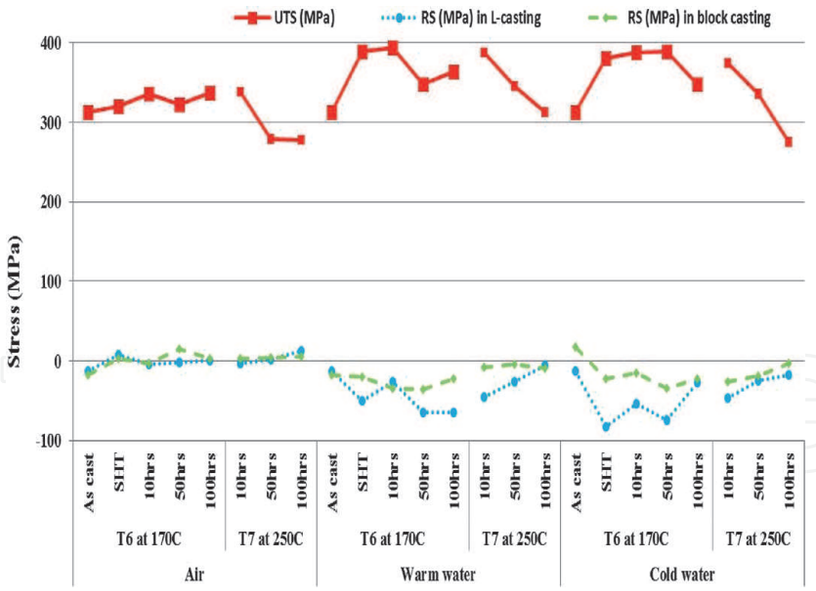

Figure 10.
Variation of tensile stresses and residual stresses in B319.1, as a function of different working parameters.

mechanical strength at lower solidification rates. Finally, the levels of residual stress are markedly reduced because of stress dissipation through the dislocation glide mechanism.

Figure 10 summarizes the ultimate tensile stress (UTS) and residual stress (RS) values obtained for the B319.1 alloy, as a function of different working parameters and quenching media. The figure demonstrates that material with higher strength, as in the case of B319.1 alloy, produces higher residual stresses (compared to 356 alloy under same heat treatment conditions [24]). It also shows that there is direct proportionality between UTS and RS with quenching rate. The relaxation of residual stresses is significantly dependent on aging temperature and proceeds smoothly with the increase in aging time. A significant increase in the residual stresses is observed in specimens with low SDAS, as in the L-shaped casting, while lower residual stresses are measured in specimens obtained from the block casting, with high SDAS.

3.2 Stage II: influence of working parameters on the development of stresses in I4 and V-6 engine blocks

Microstructural analysis was carried out using optical microscopy to observe the dendrite structure in both I4 and V6 engine blocks at different locations. Optical microscopy revealed a variation in the dendritic structure along the length of the cylinder bridge region of both I-4 and V-6 engine blocks. It was observed that the top of the cylinder bridge contained relatively coarse dendrites, while the bottom of the cylinder contained finer dendrites, **Figure 11**.

The secondary dendrite arm spacing (SDAS) was measured at the top and bottom regions of the cylinder bridges. The average SDAS was found to decrease from 57 to 40 μm for the I-4 engine block, and from 41 to 21 μm in the case of the V6 engine block. For both types of engine blocks, the SDAS results for the bottom region of the cylinder bridge indicate a shorter solidification time, i.e. a higher cooling rate compared to the top region of the cylinder bridge [37].

Figure 12(a) and **(b)** illustrate partial spheroidization of Si eutectic phase after the application of solution heat treatment. However, full modification of the Al-Si eutectic was not observed since the modified B319.1 alloy used in engine block

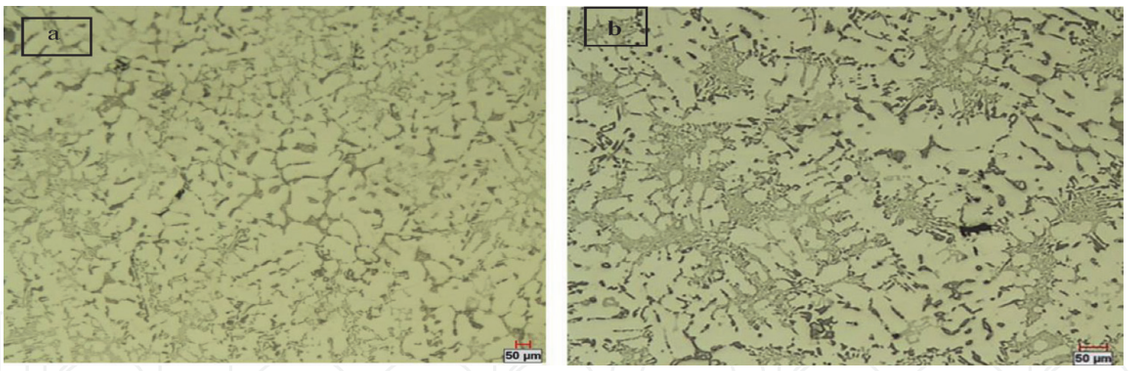

Figure 11.
Optical micrographs showing the dendrite structure of (a) top region of I-4 engine and (b) top region of V-6 engine.

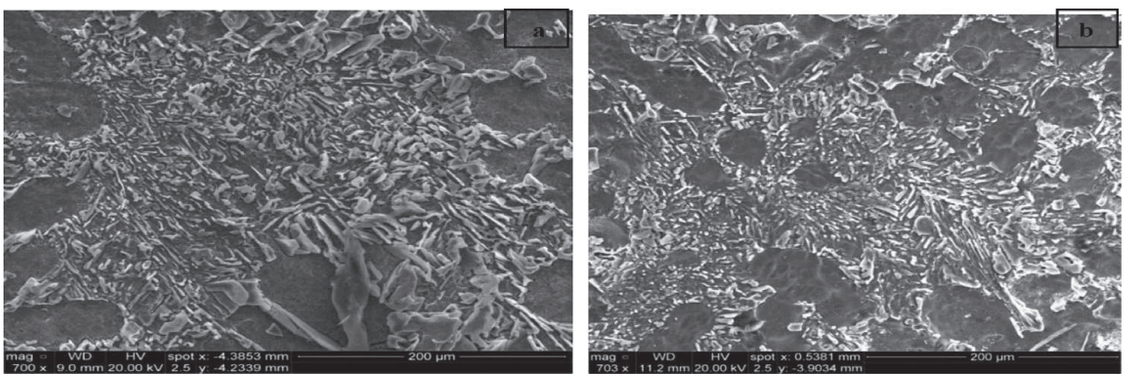

Figure 12.
Optical micrographs showing Si morphology in I4-engine blocks: (a) as received and (b) 8 h solution treatment at 500°C condition.

production, contained a larger amount of Si than the standard 319 alloy [38]. To reach full modification of the Al-Si eutectic, larger additions of Sr., longer heat treatment times, and higher cooling rates would be required. **Figure 13** demonstrated the actual size and density of the precipitates obtained after T6 and T7 aging treatments, for aging times of 10 and 100 hours. As may be seen, at the T7 aging temperature of 250°C, the precipitates are coarser, rod-like in shape, and spread further apart after 100 hours aging time, compared to what is observed at the T6 aging temperature of 170°C.

3.3 Distortion of an engine block is inevitable with time due to the presence of residual stresses

The distortion may either be a product of thermal growth or the product of tensile residual stresses that exceed the yield stress of the block material or alloy. Thermal growth means changes in volume related to phase transformation during heat treatment of the alloy. In case of thermal growth, it is found that the T7 treatment offers the best dimensional stability over T4 and T6 treatments as it produces the stable θ (Al_2Cu), phase which has a lower specific volume when compared to θ' (Al_2Cu) neglecting the effect of thermal growth distortion [39]. Such distortion may occur through the introduction of excessive residual stresses. When theses residual stresses exceed the yield stress of the material, distortion occurs [40].

The residual stresses in the I-4 engine blocks in the as-cast, air cooled, and air cooled + freezing conditions (−30°C) were 100, 70, and 50 MPa, respectively. These results indicate that the SHT process partially relieved some of the tensile

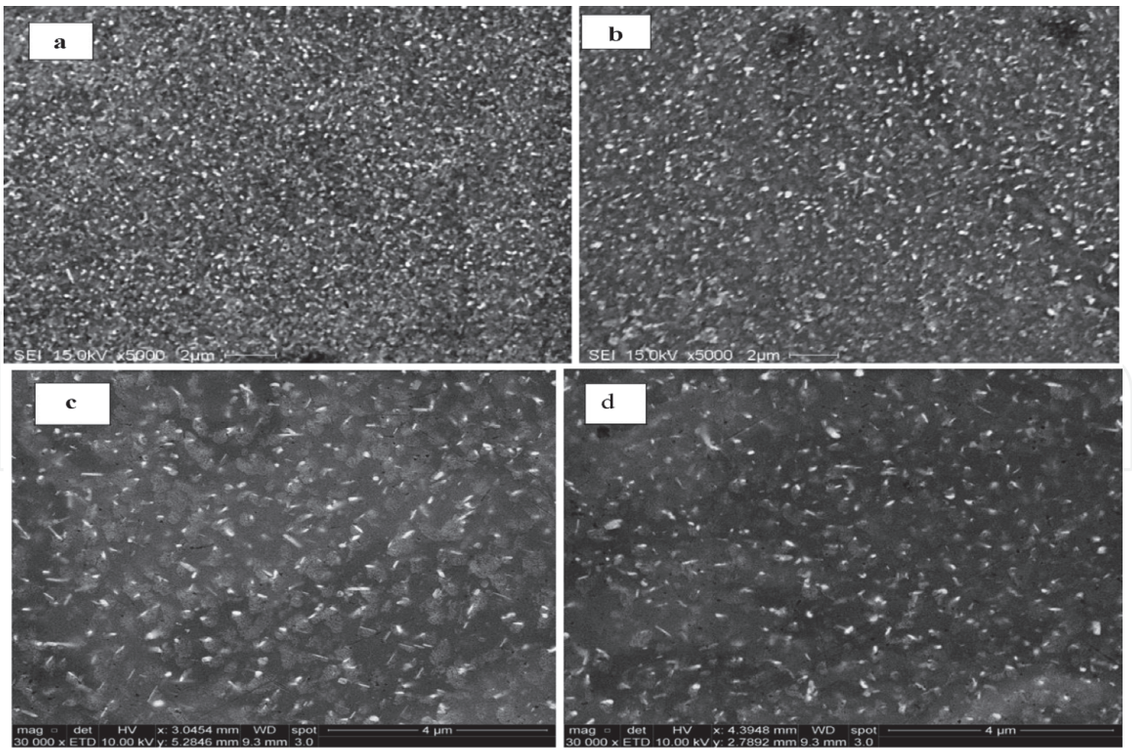

Figure 13.
Backscattered electron images of the size and density of the precipitates in I-4 engine block: (a) after aging at 170°C for 10 hours; (b) after aging at 170°C for 100 hours (c) after aging at 250°C for 10 hours; (d) after aging at 250°C for 100 hours.

residual stresses which evolved in the Al-cylinder bridge region, with a subsequent reduction when freezing was performed through the operation. **Figure 14** reveals that there is significant relieving of residual stresses ongoing from the as-cast and to the SHT condition where these residual stresses are relieved by 25, 75, and 65%, respectively, when subjected to air cooling, warm water quenching and cold-water quenching. This trend indicates that SHT plays an important role in the relieving of residual stresses. Previous research studies [10, 41] concluded that residual stresses can be relieved thermally either instantaneously, when locked-in stresses exceed the yield strength or gradually through creep mechanisms.

At slow cooling rates, there is no significant difference in cooling rates between aluminum (Al) and cast iron (CI) liners and since the aluminum contracts to a greater extent with decreasing temperature, large residual stresses are developed due to the thermo-mechanical mismatch between the two materials resulting from the hindrance of free contraction of the aluminum. On the other hand, at high cooling rates such as when the blocks are quenched in water, the CI liners cool at very high rates similar to the surrounding aluminum. This leads to the contraction

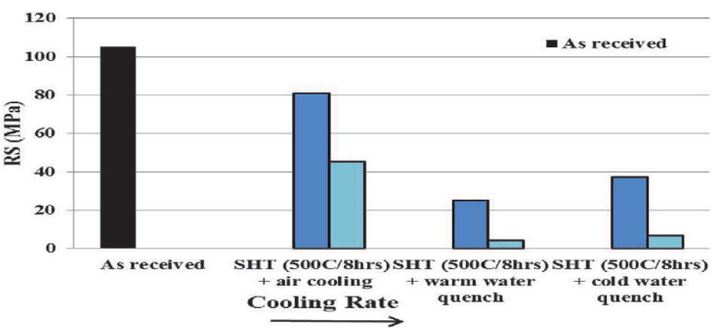

Figure 14.
Residual stress development at different quenching/cooling rates.

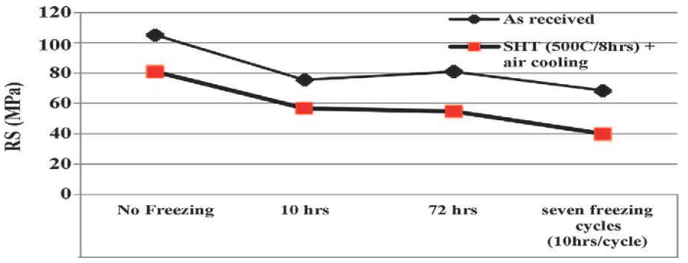

Figure 15.
Effect of stable vs. cyclic freezing on the development of residual stresses.

of both Al and CI liners at similar rates, reducing the thermo-mechanical mismatch between them, resulting in much lower stresses inside the engine blocks.

Freezing after quenching is considered one of the techniques which can be used to further reduce the amount of residual stresses by reversing the pattern of thermal gradient imposed during solution heat treatment. Despite the benefits of cryogenic treatment on both mechanical properties and the residual stresses developed in ferrous alloys, there are few reports in the literature related to the freezing treatment of nonferrous materials and the consequent effect on residual stress and mechanical properties [32, 34].

Figure 15 illustrates the effect of freezing on the development of residual stresses. At least 20% reduction in residual stresses after the implementation of the freezing process is noted, which supports the effectiveness of the freezing

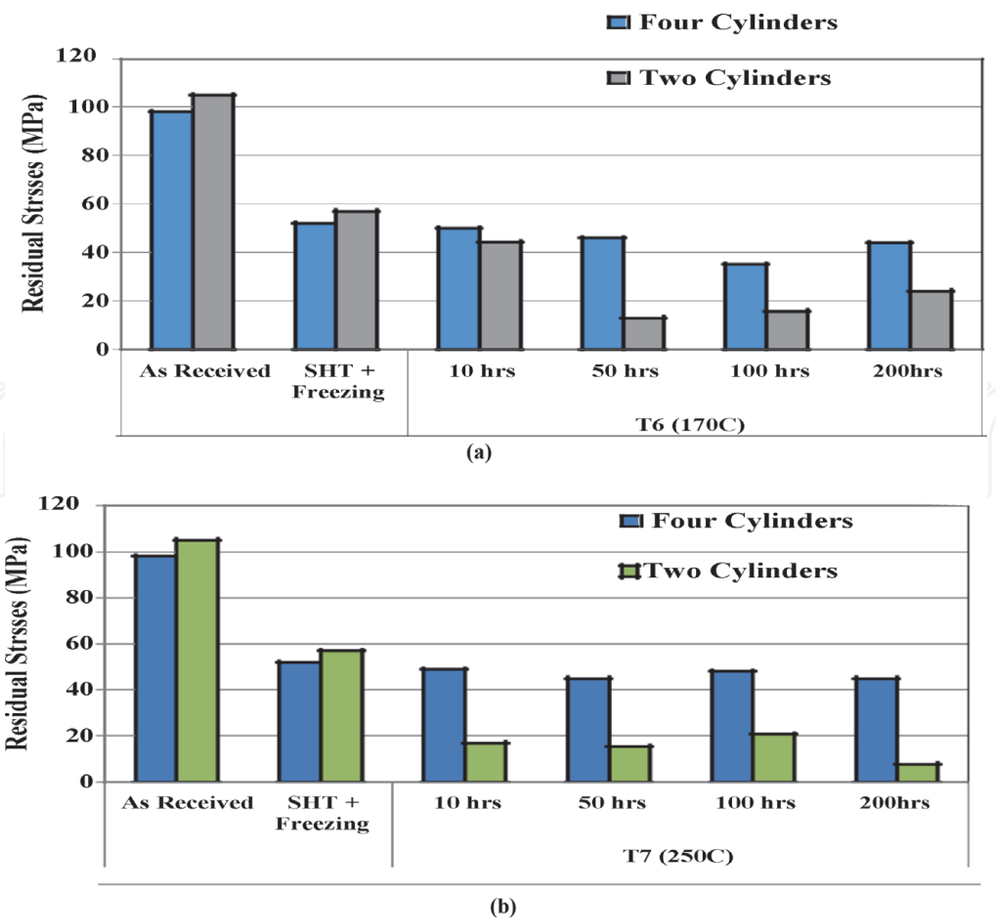

Figure 16.
Effect of freezing and aging on the development of residual stresses in two- and four-cylinder engine blocks: (a) T6 at 170°C and (b) T7 at 250°C.

treatment. Increasing the freezing time has no significant effect on controlling the residual stresses, as may be seen from **Figure 15**, around 30% reduction in residual stresses is observed after stable freezing despite prolonged exposure to freezing. Reduction in residual stresses reaches 45% after cyclic freezing. However, for most of the current study, stable freezing rather than cyclic freezing was used, where the samples were exposed to −30°C for 24 hours, for reasons of cost efficiency and easy handling associated with the process. This method may be considered as a "shallow" cryogenic treatment, as the freezing was extended to only −30°C (compared to temperatures of – 100°C used in industrial cryogenic treatments) (**Figure 16**).

4. Conclusions

Based on the obtained data, the present conclusions may be drawn.

4.1 Stage I

1. Results obtained for B319.1 alloy indicate that highest residual stresses are obtained after quenching in cold water whereas in all condition,

2. Air quenching produces no significant residual stresses.

3. Stress relieving treatments (T6 and T7) lead to the relaxation of residual stresses.

4. Also, the rate of relaxation increases with increasing temperature and time.

5. Significant increase in the residual stresses is observed in specimens with lower SDAS.

6. Thus, SDAS has a significant effect on the evolution of residual stresses.

4.2 Stage II

1. After quenching, the residual stresses evolved in engine blocks are the same either for the whole block (four cylinders) or for the sectioned half-block (two cylinders).

2. Solution heat treatment and freezing (cryogenic treatment) maximizes the amount of residual stress relaxation where 50% of the residual stresses were reduced after the solution heat treatment step.

3. With freezing, around 30% of residual stress relaxation may be obtained. Increasing the freezing time or the use of cyclic freezing has no significant effect on relieving the residual stress.

4. In spite of the effect of quenching rate, residual stresses are gradually relaxed till they reach the limit at 20 MPa. Two-cylinder engine blocks undergo greater residual stress relaxation after aging compared to that observed in four-cylinder engine blocks.

Author details

Serageldin Salem Mohamed[1], Agnes M. Samuel[1], Herbert W. Doty[2], Salvador Valtierra[3] and Fawzy H. Samuel[1*]

1 Université du Québec à Chicoutimi, Chicoutimi, Québec, Canada

2 General Motors Materials Engineering, Pontiac, MI, USA

3 Corporativo Nemak, Garza Garcia, NL, Mexico

*Address all correspondence to: fhsamuel@uqac.ca

References

[1] Withers PJ. Residual stress and its role in failure. Reports on Progress in Physics. 2007;**70**(12):2211-2264

[2] Dieter GE, Bacon D. Mechanical Metallurgy. Vol. 3. New York: McGraw-Hill; 1986

[3] Lombardi A et al. Determining the mechanism of in-service cylinder distortion in aluminum engine blocks with cast-in gray iron liners. Metallurgical and Materials Transactions A: Physical Metallurgy and Materials Science. 2014;**45A**(13): 6291-6303

[4] Prasad P. Characterization of New, Cast, High Temperature Aluminum Alloys for Diesel Engine Applications. Cincinnati, OH: University of Cincinnati; 2006

[5] Lenny J. Jr. Replacing the cast iron liners for aluminum engine cylinder blocks: A comparative assessment of potential candidates [engineering thesis submitted to graduate]. Hartford, Connecticut: Faculty of Rensselaer Polytechnic Institute; 2011

[6] Wang Q et al. Methods of predicting residual stresses and distortion in quenched aluminum castings. Google Patents; 2012

[7] Wang Q et al. Modeling of residual stresses in aluminum castings. In: 117th Metalcasting Congress. Schaumberg, IL: AFS Inc.; 2013

[8] Montazersadgh FH, Fatemi A. Stress Analysis and Optimization of Crankshafts Subject to Dynamic Loading. Toledo, OH: The University of Toledo; 2007

[9] Wang Q, Chang C, Zhang G, Paluch D. Modeling of residual stresses in quenched cast aluminum components. SAE International Journal of Materials and Manufacturing. 2011;**4**(1):844-852. DOI: 10.4271/2011-01-0539

[10] Lados DA, Apelian D, Wang L. Minimization of residual stress in heat-treated Al–Si–Mg cast alloys using uphill quenching: Mechanisms and effects on static and dynamic properties. Materials Science and Engineering A. 2010;**527** (13–14):3159-3165

[11] Carrera E et al. Measurement of residual stresses in cast aluminium engine blocks. Journal of Materials Processing Technology. 2007;**189**(1): 206-210

[12] Lombardi A. A study of cylinder bore distortion in V6 aluminum alloy engine block. In: Mechanical Engineering. Toronto, ON: Ryerson University; 2011

[13] Carrera E et al. Study of residual stresses in complex aluminium castings. International Journal of Cast Metals Research. 2012;**25**(5):264-269

[14] Colas R, Rodríguez A, Talamantes J, Valtierra S. Solidification analysis of aluminium engine block. International Journal of Cast Metals Research. 2004; **17**:332-338

[15] Elmquist L, Brehmer A, Schmidt P, Israelsson B. Residual stresses in cast iron components – Simulated results verified by experimental, measurements. Materials Science Forum Submitted. 2017;**925**:326-333

[16] Rossini N et al. Methods of measuring residual stresses in components. Materials and Design. 2012;**35**:572-588

[17] Tavitas-Medrano FJ et al. Effect of Mg and Sr-modification on the mechanical properties of 319-type aluminum cast alloys subjected to

artificial aging. Materials Science and Engineering A. 2008;**480**(1–2):356-364

[18] Elsebaie O et al. The role of alloying additives and aging treatment on the impact behavior of 319 cast alloy. Materials & Design. 2011;**32**(6): 3205-3220

[19] Han Y et al. Optimizing the tensile properties of Al–Si–Cu–Mg 319-type alloys: Role of solution heat treatment. Materials & Design. 2014;**58**(0):426-438

[20] García-García G, Espinoza-Cuadra J, Mancha-Molinar H. Copper content and cooling rate effects over second phase particles behavior in industrial aluminum–silicon alloy 319. Materials & Design. 2007;**28**(2):428-433

[21] Torsten EM, Staab D, Folegati P, Wolfertz I, Puska MJ. Stability of Cu-precipitates in Al-Cu alloys. Applied Sciences. 2018;**8**:1003. DOI: 10.3390/app8061003

[22] Guinier A. La diffraction de rayon X aux tres petis angles: Application a l'etude de phenomenes ultramicroscopiques. Ann. Phys. 1938; **12**:161-237

[23] Preston G. The diffraction of X-rays by an age-hardening aluminum and copper alloys. Proceedings of the Royal Society of London. Series A, Mathematical and Physical Sciences. 1938;**167**:526-538

[24] Ibrahim MF, Samuel AM, Doty HW, Samuel FH. Effect of aging conditions on precipitation hardening in Al–Si–Mg and Al–Si–Cu–Mg alloys. International Journal of Metalcasting. 2017;**11**(2):274-286

[25] Ratke L, Voorhees PW. Growth and Coarsening: Ostwald Ripening in Material Processing. Berlin, Germany: Springer Science & Business Media; 2013

[26] Voorhees PW. The theory of Ostwald ripening. Journal of Statistical Physics. 1985;**38**(1):231-252

[27] Gladman T. Precipitation hardening in metals. Materials Science and Technology. 1999;**15**(1):30-36

[28] Ogris E. Development of Al-Si-Mg Alloys for Semi-Solid Processing and Silicon Spheroidization Treatment (SST) for Al-Si-Cast Alloys. Zurich, Switzerland: ETH; 2002

[29] Santos-Güemes R, Bellón B, Esteban-Manzanares G, Segurado J, Capolungo L, LLorca J. Multiscale modelling of precipitation hardening in Al–Cu alloys: Dislocation dynamics simulations and experimental validation. Acta Materialia. 2020;**188**:475-485

[30] Kleiven D, Akola J. Precipitate formation in aluminium alloys: Multi-scale modelling approach. Acta Materialia. 2020;**195**:123-131

[31] Furukawa M, Horita Z, Nemoto M, Valiev RZ. Microhardness measurements and the Hall-Petch relationship in an Al-Mg alloy with submicrometer grain size. Acta Materialia. 1996;**44**:4619-4629

[32] Withers PJ, Bhadeshia H. Residual stress. Part 2–Nature and origins. Materials Science and Technology. 2001;**17**(4):366-375

[33] Withers PJ, Bhadeshia H. Residual stress. Part 1–Measurement techniques. Materials Science and Technology. 2001;**17**(4):355-365

[34] Robinson J, Tanner D, Truman C. 50th anniversary article: The origin and management of residual stress in heat-treatable aluminium alloys. Strain. 2014; **50**(3):185-207

[35] Hunsicker HY. Dimensional changes in heat treating aluminum alloys.

Metallurgical Transactions A. 1980; **11**(5):759-773

[36] James M. Relaxation of residual stresses an overview. In: Advances in Surface Treatments. Technology–Applications–Effects. Vol. 4. Oxford, UK: Pergamon Press; 1987. pp. 349-365

[37] Wang Q. Microstructural effects on the tensile and fracture behavior of aluminum casting alloys A356/357. Metallurgical and Materials Transactions A. 2003;**34**:2887-2899

[38] Bäckerud L, Chai G, Tamminen J. Solidification Characteristics of Aluminum Alloys. Vol. 2: Foundry Alloys. Des Plaines, IL: AFS/SKANALUMINIUM; 1990

[39] Godlewski LA et al. The effect of aging on the relaxation of residual stress in cast aluminum. Metallurgical and Materials Transactions A. 2013;**44**(10): 4809-4818

[40] Wiesner D et al. Residual stress measurements of cast aluminum engine blocks using diffraction. Advances in X-Ray Analysis. 2005;**48**:136-142

[41] Araghchi M, Mansori H, Vafaei R, Gou Y. A novel cryogenic treatment for reduction of residual stresses in 2024 aluminum alloy. Materials Science and Engineering A. 2017;**689**:48-52